

SUSY QCD corrections to Higgs- b Production: Is the Δ_b Approximation Accurate?

S. Dawson^a, C. B. Jackson^b, P. Jaiswal^{a,c}

^a*Department of Physics, Brookhaven National Laboratory, Upton, NY 11973, USA*

^b*Physics Department, University of Texas, Arlington, Texas*

^c*Yang Institute for Theoretical Physics,
Stony Brook University, Stony Brook, NY 11790, USA*

Abstract

The associated production of a Higgs boson with a b quark is a discovery channel for the lightest MSSM neutral Higgs boson. We consider the SUSY QCD contributions from squarks and gluinos and discuss the decoupling properties of these effects. A detailed comparison of our exact $\mathcal{O}(\alpha_s)$ results with those of a widely used effective Lagrangian approach, the Δ_b approximation, is presented. The Δ_b approximation is shown to accurately reproduce the exact one-loop SQCD result to within a few percent over a wide range of parameter space.

I. INTRODUCTION

Once a light Higgs-like particle is discovered it will be critical to determine if it is the Higgs Boson predicted by the Standard Model. The minimal supersymmetric Standard Model (MSSM) presents a comparison framework in which to examine the properties of a putative Higgs candidate. The MSSM Higgs sector contains 5 Higgs bosons—2 neutral bosons, h and H , a pseudoscalar boson, A , and 2 charged bosons, H^\pm . At the tree level the theory is described by just 2 parameters, which are conveniently chosen to be M_A , the mass of the pseudoscalar boson, and $\tan\beta$, the ratio of vacuum expectation values of the 2 neutral Higgs bosons. Even when radiative corrections are included, the theory is highly predictive[1–3].

In the MSSM, the production mechanisms for the Higgs bosons can be significantly different from in the Standard Model. For large values of $\tan\beta$, the heavier Higgs bosons, A and H , are predominantly produced in association with b quarks. Even for $\tan\beta \sim 5$, the production rate in association with b quarks is similar to that from gluon fusion for A and H production[19]. For the lighter Higgs boson, h , for $\tan\beta \gtrsim 7$ the dominant production mechanism at both the Tevatron and the LHC is production with b quarks for light M_A ($\lesssim 200$ GeV), where the $b\bar{b}h$ coupling is enhanced. Both the Tevatron[4] and the LHC experiments[5] have presented limits Higgs production in association with b quarks, searching for the decays $h \rightarrow \tau^+\tau^-$ and $b\bar{b}^1$. These limits are obtained in the context of the MSSM are sensitive to the b -squark and gluino loop corrections which we consider here.

The rates for bh associated production at the LHC and the Tevatron have been extensively studied[8–18] and the NLO QCD correction are well understood, both in the 4- and 5-flavor number parton schemes[9, 11, 15]. In the 4- flavor number scheme, the lowest order processes for producing a Higgs boson and a b quark are $gg \rightarrow b\bar{b}h$ and $q\bar{q} \rightarrow b\bar{b}h$ [8, 12, 17]. In the 5- flavor number scheme, the lowest order process is $bg \rightarrow bh$ ($\bar{b}g \rightarrow \bar{b}h$). The two schemes represent different orderings of perturbation theory and calculations in the two schemes produce rates which are in qualitative agreement[11, 19]. In this paper, we use the 5-flavor number scheme for simplicity. The resummation of threshold logarithms[20], electroweak corrections[21, 22] and SUSY QCD corrections[23] have also been computed for

¹ The expected sensitivities of ATLAS and CMS to b Higgs associated production are described in Refs. [6, 7].

bh production in the 5– flavor number scheme.

Here, we focus on the role of squark and gluino loops. The properties of the SUSY QCD corrections to the $b\bar{b}h$ vertex, both for the decay $h \rightarrow b\bar{b}$ [24–27] and the production, $b\bar{b} \rightarrow h$ [12, 27–29], were computed long ago. The contributions from b squarks and gluinos to the lightest MSSM Higgs boson mass are known at 2-loops[30, 31], while the 2-loop SQCD contributions to the $b\bar{b}h$ vertex is known in the limit in which the Higgs mass is much smaller than the squark and gluino masses[32, 33]. The contributions of squarks and gluinos to the on-shell $b\bar{b}h$ vertex are non-decoupling for heavy squark and gluino masses and decoupling is only achieved when the pseudoscalar mass, M_A , also becomes large.

An effective Lagrangian approach, the Δ_b approximation[25, 26], can be used to approximate the SQCD contributions to the on-shell $b\bar{b}h$ vertex and to resum the $(\alpha_s \tan \beta / M_{SUSY})^n$ enhanced terms. The numerical accuracy of the Δ_b effective Lagrangian approach has been examined for a number of cases. The 2–loop contributions to the lightest MSSM Higgs boson mass of $\mathcal{O}(\alpha_b \alpha_s)$ were computed in Refs. [30] and [31], and it was found that the majority of these corrections could be absorbed into a 1–loop contribution by defining an effective b quark mass using the Δ_b approach. The sub-leading contributions to the Higgs boson mass (those not absorbed into Δ_b) are then of $\mathcal{O}(1 \text{ GeV})$. The Δ_b approach also yields an excellent approximation to the SQCD corrections for the decay process $h \rightarrow b\bar{b}$ [27]. It is particularly interesting to study the accuracy of the Δ_b approximation for production processes where one of the b quarks is off-shell. The SQCD contributions from squarks and gluinos to the inclusive Higgs production rate in association with b quarks has been studied extensively in the 4FNS in Ref. [37], where the the lowest order contribution is $gg \rightarrow b\bar{b}h$. In the 4FNS, the inclusive cross section including the exact 1-loop SQCD corrections is reproduced to within a few percent using the Δ_b approximation. However, the accuracy of the Δ_b approximation for the MSSM neutral Higgs boson production in the 5FNS has been studied for only a small set of MSSM parameters in Ref. [23]. The major new result of this paper is a detailed study of the accuracy of the Δ_b approach in the 5FNS for the $bg \rightarrow bh$ production process. In this case, one of the b quarks is off-shell and there are contributions which are not contained in the effective Lagrangian approach.

The plan of the paper is as follows: Section 2 contains a brief review of the MSSM Higgs and b squark sectors and also a review of the effective Lagrangian approximation. The calculation of Ref. [23] is summarized in Section 2. We include SQCD contributions to

bh production which are enhanced by $m_b \tan \beta$ which were omitted in Ref. [23]. Analytic results for the SQCD corrections to $bg \rightarrow bh$ in the extreme mixing scenarios in the b squark sector are presented in Section 3. Section 4 contains numerical results for the $\sqrt{s} = 7$ TeV LHC. Finally, our conclusions are summarized in Section 5. Detailed analytic results are relegated to a series of appendices.

II. BASICS

A. MSSM Framework

In the simplest version of the MSSM there are two Higgs doublets, H_u and H_d , which break the electroweak symmetry and give masses to the W and Z gauge bosons. The neutral Higgs boson masses are given at tree level by,

$$M_{h,H}^2 = \frac{1}{2} \left[M_A^2 + M_Z^2 \mp \sqrt{(M_A^2 + M_Z^2)^2 - 4M_A^2 M_Z^2 \cos^2 2\beta} \right], \quad (1)$$

and the angle, α , which diagonalizes the neutral Higgs mass is

$$\tan 2\alpha = \tan 2\beta \left(\frac{M_A^2 + M_Z^2}{M_A^2 - M_Z^2} \right). \quad (2)$$

In practice, the relations of Eqs. 1 and 2 receive large radiative corrections which must be taken into account in numerical studies. We use the program FeynHiggs[34–36] to generate the Higgs masses and an effective mixing angle, α_{eff} , which incorporates higher order effects.

The scalar partners of the left- and right- handed b quarks, \tilde{b}_L and \tilde{b}_R , are not mass eigenstates, but mix according to,

$$L_M = -(\tilde{b}_L^*, \tilde{b}_R^*) M_b^2 \begin{pmatrix} \tilde{b}_L \\ \tilde{b}_R \end{pmatrix}. \quad (3)$$

The \tilde{b} squark mass matrix is,

$$M_b^2 = \begin{pmatrix} \tilde{m}_L^2 & m_b X_b \\ m_b X_b & \tilde{m}_R^2 \end{pmatrix}, \quad (4)$$

and we define,

$$\begin{aligned} X_b &= A_b - \mu \tan \beta \\ \tilde{m}_L^2 &= M_Q^2 + m_b^2 + M_Z^2 \cos 2\beta (I_3^b - Q_b \sin^2 \theta_W) \\ \tilde{m}_R^2 &= M_D^2 + m_b^2 + M_Z^2 \cos 2\beta Q_b \sin^2 \theta_W. \end{aligned} \quad (5)$$

$M_{Q,D}$ are the soft SUSY breaking masses, $I_3^b = -1/2$, and $Q_b = -1/3$. The parameter A_b is the trilinear scalar coupling of the soft supersymmetry breaking Lagrangian and μ is the Higgsino mass parameter. The b squark mass eigenstates are \tilde{b}_1 and \tilde{b}_2 and define the b -squark mixing angle, $\tilde{\theta}_b$

$$\begin{aligned}\tilde{b}_1 &= \cos \tilde{\theta}_b \tilde{b}_L + \sin \tilde{\theta}_b \tilde{b}_R \\ \tilde{b}_2 &= -\sin \tilde{\theta}_b \tilde{b}_L + \cos \tilde{\theta}_b \tilde{b}_R.\end{aligned}\tag{6}$$

At tree level,

$$\sin 2\tilde{\theta}_b = \frac{2m_b(A_b - \mu \tan \beta)}{M_{\tilde{b}_1}^2 - M_{\tilde{b}_2}^2}\tag{7}$$

and the sbottom mass eigenstates are,

$$M_{\tilde{b}_1, \tilde{b}_2}^2 = \frac{1}{2} \left[\tilde{m}_L^2 + \tilde{m}_R^2 \mp \sqrt{(\tilde{m}_L^2 - \tilde{m}_R^2)^2 + 4m_b^2 X_b^2} \right].\tag{8}$$

B. Δ_b Approximation: The Effective Lagrangian Approach

Loop corrections which are enhanced by powers of $\alpha_s \tan \beta$ can be included in an effective Lagrangian approach. At tree level, there is no $\bar{\psi}_L b_R H_u$ coupling in the MSSM, but such a coupling arises at one loop and gives an effective interaction[25–27]²,

$$L_{eff} = -\lambda_b \bar{\psi}_L \left(H_d + \frac{\Delta_b}{\tan \beta} H_u \right) b_R + h.c. \quad .\tag{9}$$

Eq. 9 shifts the b quark mass from its tree level value,³

$$m_b \rightarrow \frac{\lambda_b v_1}{\sqrt{2}} (1 + \Delta_b),\tag{10}$$

and also implies that the Yukawa couplings of the Higgs bosons to the b quark are shifted from the tree level predictions. This shift of the Yukawa couplings can be included with an effective Lagrangian approach[26, 27],

$$L_{eff} = -\frac{m_b}{v_{SM}} \left(\frac{1}{1 + \Delta_b} \right) \left(-\frac{\sin \alpha}{\cos \beta} \right) \left(1 - \frac{\Delta_b}{\tan \beta \tan \alpha} \right) \bar{b} b h.\tag{11}$$

The Lagrangian of Eq. 11 has been shown to sum all terms of $\mathcal{O}(\alpha_s \tan \beta)^n$ for large $\tan \beta$ [25, 26].⁴ This effective Lagrangian has been used to compute the SQCD corrections

² The neutral components of the Higgs bosons receive vacuum expectation values: $\langle H_d^0 \rangle = \frac{v_1}{\sqrt{2}}$, $\langle H_u^0 \rangle = \frac{v_2}{\sqrt{2}}$.

³ $v_{SM} = (\sqrt{2}G_F)^{-1/2}$, $v_1 = v_{SM} \cos \beta$

⁴ It is also possible to sum the contributions which are proportional to A_b , but these terms are less important numerically[27].

to both the inclusive production process, $b\bar{b} \rightarrow h$, and the decay process, $h \rightarrow b\bar{b}$, and yields results which are within a few percent of the exact one-loop SQCD calculations[27, 37].

The expression for Δ_b is found in the limit $m_b \ll M_h, M_Z \ll M_{\tilde{b}_1}, M_{\tilde{b}_2}, M_{\tilde{g}}$. The 1-loop contribution to Δ_b from sbottom/gluino loops is[25, 26, 38]

$$\Delta_b = \frac{2\alpha_s(\mu_S)}{3\pi} M_{\tilde{g}} \mu \tan \beta I(M_{\tilde{b}_1}, M_{\tilde{b}_2}, M_{\tilde{g}}), \quad (12)$$

where the function $I(a, b, c)$ is,

$$I(a, b, c) = \frac{1}{(a^2 - b^2)(b^2 - c^2)(a^2 - c^2)} \left\{ a^2 b^2 \log\left(\frac{a^2}{b^2}\right) + b^2 c^2 \log\left(\frac{b^2}{c^2}\right) + c^2 a^2 \log\left(\frac{c^2}{a^2}\right) \right\}, \quad (13)$$

and $\alpha_s(\mu_S)$ should be evaluated at a typical squark or gluino mass. The 2-loop QCD corrections to Δ_b have been computed and demonstrate that the appropriate scale at which to evaluate Δ_b is indeed of the order of the heavy squark and gluino masses[32, 33]. The renormalization scale dependence of Δ_b is minimal around $\mu_0/3$, where $\mu_0 \equiv (M_{\tilde{g}} + m_{\tilde{b}_1} + m_{\tilde{b}_2})/3$. In our language this is a high scale, of order the heavy SUSY particle masses. The squarks and gluinos are integrated out of the theory at this high scale and their effects contained in Δ_b . The effective Lagrangian is then used to calculate light Higgs production at a low scale, which is typically the electroweak scale, $\sim 100 \text{ GeV}$.

Using the effective Lagrangian of Eq. 9, which we term the Improved Born Approximation (or Δ_b approximation), the cross section is written in terms of the effective coupling,

$$g_{bbh}^{\Delta_b} \equiv g_{bbh} \left(\frac{1}{1 + \Delta_b} \right) \left(1 - \frac{\Delta_b}{\tan \beta \tan \alpha} \right), \quad (14)$$

where

$$g_{bbh} = - \left(\frac{\sin \alpha}{\cos \beta} \right) \frac{\overline{m}_b(\mu_R)}{v_{SM}}. \quad (15)$$

We evaluate $\overline{m}_b(\mu_R)$ using the 2-loop \overline{MS} value at a scale μ_R of $\mathcal{O}(M_h)$, and use the value of α_{eff} determined from FeynHiggs. The Improved Born Approximation consists of rescaling the tree level cross section, σ_0 , by the coupling of Eq. 14⁵,

$$\sigma_{IBA} = \left(\frac{g_{bbh}^{\Delta_b}}{g_{bbh}} \right)^2 \sigma_0. \quad (16)$$

The Improved Born Approximation has been shown to accurately reproduce the full SQCD calculation of $pp \rightarrow \bar{t}bH^+$ [39, 40].

⁵ This is the approximation used in Ref. [19] to include the SQCD corrections.

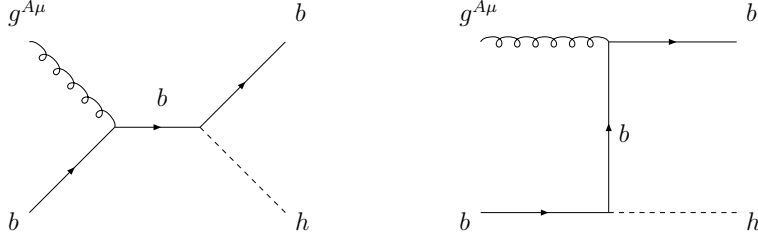


FIG. 1: Feynman diagrams for $g(q_1) + b(q_2) \rightarrow b(p_b) + h(p_h)$.

The one-loop result including the SQCD corrections for $bg \rightarrow bh$ can be written as,

$$\sigma_{SQCD} \equiv \sigma_{IBA} \left(1 + \Delta_{SQCD} \right), \quad (17)$$

where Δ_{SQCD} is found from the exact SQCD calculation summarized in Appendix B.

The Improved Born Approximation involves making the replacement in the tree level Lagrangian,

$$m_b \rightarrow \frac{m_b}{1 + \Delta_b}. \quad (18)$$

Consistency requires that this substitution also be made in the squark mass matrix of Eq. 4[41, 42]

$$M_b^2 \rightarrow \begin{pmatrix} \tilde{m}_L^2 & \left(\frac{m_b}{1 + \Delta_b} \right) X_b \\ \left(\frac{m_b}{1 + \Delta_b} \right) X_b & \tilde{m}_R^2 \end{pmatrix}. \quad (19)$$

The effects of the substitution of Eq. 18 in the b -squark mass matrix are numerically important, although they generate contributions which are formally higher order in α_s . Eqs. 12 and 19 can be solved iteratively for $M_{\tilde{b}_1}$, $M_{\tilde{b}_2}$ and Δ_b using the procedure of Ref. [41]⁶.

C. SQCD Contributions to $gb \rightarrow bh$

The contributions from squark and gluino loops to the $gb \rightarrow bh$ process have been computed in Ref. [23] in the $m_b = 0$ limit. We extend that calculation by including terms which are enhanced by $m_b \tan \beta$ and provide analytic results in several useful limits.

The tree level diagrams for $g(q_1) + b(q_2) \rightarrow b(p_b) + h(p_h)$ are shown in Fig. 1. We define

⁶ We use FeynHiggs only for calculating M_h and $\sin \alpha_{eff}$.

the following dimensionless spinor products

$$\begin{aligned}
M_s^\mu &= \frac{\bar{u}(p_b) (\not{q}_1 + \not{q}_2) \gamma^\mu u(q_2)}{s} \\
M_t^\mu &= \frac{\bar{u}(p_b) \gamma^\mu (\not{p}_b - \not{q}_1) u(q_2)}{t} \\
M_1^\mu &= q_2^\mu \frac{\bar{u}(p_b) u(q_2)}{u} \\
M_2^\mu &= \frac{\bar{u}(p_b) \gamma^\mu u(q_2)}{m_b} \\
M_3^\mu &= p_b^\mu \frac{\bar{u}(p_b) \not{q}_1 u(q_2)}{m_b t} \\
M_4^\mu &= q_2^\mu \frac{\bar{u}(p_b) \not{q}_1 u(q_2)}{m_b s}, \tag{20}
\end{aligned}$$

where $s = (q_1 + q_2)^2$, $t = (p_b - q_1)^2$ and $u = (p_b - q_2)^2$. In the $m_b = 0$ limit, the tree level amplitude depends only on M_s^μ and M_t^μ , and M_1^μ is generated at one-loop. When the effects of the b mass are included, M_2^μ , M_3^μ , and M_4^μ are also generated.

The tree level amplitude is

$$\mathcal{A}_{\alpha\beta}^a |_0 = -g_s g_{bbh} (T^a)_{\alpha\beta} \epsilon_\mu(q_1) \{M_s^\mu + M_t^\mu\}, \tag{21}$$

and the one loop contribution can be written as

$$\mathcal{A}_{\alpha\beta}^a = -\frac{\alpha_s(\mu_R)}{4\pi} g_s g_{bbh} (T^a)_{\alpha\beta} \sum_j X_j M_j^\mu \epsilon_\mu(q_1). \tag{22}$$

In the calculations to follow, only the non-zero X_j coefficients are listed and we neglect terms of $\mathcal{O}(m_b^2/s)$ if they are not enhanced by $\tan\beta$.

The renormalization of the squark and gluino contributions is performed in the on-shell scheme and has been described in Refs. [23, 32, 43]. The bottom quark self-energy is

$$\Sigma_b(p) = \not{p} \left(\Sigma_b^V(p^2) - \Sigma_b^A(p^2) \gamma_5 \right) + m_b \Sigma_b^S(p^2). \tag{23}$$

The b quark fields are renormalized as $b \rightarrow \sqrt{Z_b^V} b$ and $Z_b^V \equiv \sqrt{1 + \delta Z_b^V}$. The contribution from the counter-terms to the self-energy is,

$$\begin{aligned}
\Sigma_b^{\text{ren}}(p) &= \Sigma_b(p) + \delta \Sigma_b(p) \\
\delta \Sigma_b(p) &= \not{p} (\delta Z_b^V - \delta Z_b^A \gamma_5) - m_b \delta Z_b^V - \delta m_b. \tag{24}
\end{aligned}$$

Neglecting the γ_5 contribution, the renormalized self-energy is then given by

$$\Sigma_b^{\text{ren}}(p) = (\not{p} - m_b) (\Sigma_b^V(p^2) + \delta Z_b^V) + m_b \left(\Sigma_b^S(p^2) + \Sigma_b^V(p^2) - \frac{\delta m_b}{m_b} \right). \tag{25}$$

The on-shell renormalization condition implies

$$\Sigma_b^{\text{ren}}(p)|_{\not{p}=m_b} = 0 \quad (26)$$

$$\lim_{\not{p} \rightarrow m_b} \left(\frac{\Sigma_b^{\text{ren}}(p)}{\not{p} - m_b} \right) = 0. \quad (27)$$

The mass and wavefunction counter-terms are⁷

$$\begin{aligned} \frac{\delta m_b}{m_b} &= [\Sigma_b^S(p^2) + \Sigma_b^V(p^2)]_{p^2=m_b^2} \\ &= \frac{\alpha_s(\mu_R)}{3\pi} \sum_{i=1}^2 \left[(-1)^i \frac{M_{\tilde{g}}}{m_b} s_{2\tilde{b}} B_0 - B_1 \right] \left(0; M_{\tilde{g}}^2, M_{\tilde{b}_i}^2 \right) \end{aligned} \quad (28)$$

$$\begin{aligned} \delta Z_b^V &= -\Sigma_b^V(p^2)|_{p^2=m_b^2} - 2m_b^2 \frac{\partial}{\partial p^2} \left(\Sigma_b^V(p^2) + \Sigma_S(p^2) \right) |_{p^2=m_b^2} \\ &= \frac{\alpha_s(\mu_R)}{3\pi} \sum_{i=1}^2 \left[B_1 + 2m_b^2 B_1' - (-1)^i 2m_b M_{\tilde{g}} s_{2\tilde{b}} B_0' \right] \left(0; M_{\tilde{g}}^2, M_{\tilde{b}_i}^2 \right), \end{aligned} \quad (29)$$

where we consistently neglect the b quark mass if it is not enhanced by $\tan \beta$. The Passarino-Veltman functions $B_0(0; M_{\tilde{g}}^2, M_{\tilde{b}_i}^2)$ and $B_1(0; M_{\tilde{g}}^2, M_{\tilde{b}_i}^2)$ are defined in Appendix A. Using the tree level relationship of Eq. 7, the mass counterterm can be written as,

$$\frac{\delta m_b}{m_b} = \frac{2\alpha_s(\mu_R)}{3\pi} M_{\tilde{g}} A_b I(M_{\tilde{b}_1}, M_{\tilde{b}_2}, M_{\tilde{g}}) - \Delta_b - \frac{\alpha_s(\mu_R)}{3\pi} \sum_{i=1}^2 B_1(0; M_{\tilde{g}}^2, M_{\tilde{b}_i}^2). \quad (30)$$

The external gluon is renormalized as $g_\mu^A \rightarrow \sqrt{Z_3} g_\mu^A = \sqrt{1 + \delta Z_3} g_\mu^A$ and the strong coupling renormalization is $g_s \rightarrow Z_g g_s$ with $\delta Z_g = -\delta Z_3/2$. We renormalize g_s using the \overline{MS} scheme with the heavy squark and gluino contributions subtracted at zero momentum[44],

$$\delta Z_3 = -\frac{\alpha_s(\mu_R)}{4\pi} \left[\frac{1}{6} \sum_{\tilde{q}_i} \left(\frac{4\pi\mu_R^2}{M_{\tilde{q}_i}^2} \right)^\epsilon + 2 \left(\frac{4\pi\mu_R^2}{M_{\tilde{g}}^2} \right)^\epsilon \right] \frac{1}{\epsilon} \Gamma(1 + \epsilon). \quad (31)$$

In order to avoid overcounting the effects which are contained in g_{bbh}^Δ to $\mathcal{O}(\alpha_s)$, we need the additional counterterm,

$$\delta_{CT} = \Delta_b \left(1 + \frac{1}{\tan \beta \tan \alpha} \right). \quad (32)$$

The total contribution of the counterterms is,

$$\sigma_{CT} = \sigma_{IBA} \left(2\delta Z_b^V + \delta Z_3 + 2\delta Z_g + 2\frac{\delta m_b}{m_b} + 2\delta_{CT} \right) = 2\sigma_{IBA} \left(\delta Z_b^V + \frac{\delta m_b}{m_b} + \delta_{CT} \right). \quad (33)$$

The $\tan \beta$ enhanced contributions from Δ_b cancel between Eqs. 30 and 32. The expressions for the contributions to the X_i , as defined in Eq. 22, are given in Appendix B for arbitrary squark and gluino masses, and separately for each 1-loop diagram.

⁷ $s_{2\tilde{b}} \equiv \sin 2\tilde{\theta}_b$.

III. RESULTS FOR MAXIMAL AND MINIMAL MIXING IN THE b -SQUARK SECTOR

A. Maximal Mixing

The squark and gluino contributions to $bg \rightarrow bh$ can be examined analytically in several scenarios. In the first scenario,

$$|\tilde{m}_L^2 - \tilde{m}_R^2| \ll \frac{m_b}{1 + \Delta_b} |X_b|. \quad (34)$$

We expand in powers of $\frac{|\tilde{m}_L^2 - \tilde{m}_R^2|}{m_b X_b}$. In this case the sbottom masses are nearly degenerate,

$$M_S^2 \equiv \frac{1}{2} \left[M_{\tilde{b}_1}^2 + M_{\tilde{b}_2}^2 \right] \\ |M_{\tilde{b}_1}^2 - M_{\tilde{b}_2}^2| = \left(\frac{2m_b |X_b|}{1 + \Delta_b} \right) \left(1 + \frac{(\tilde{m}_L^2 - \tilde{m}_R^2)^2 (1 + \Delta_b)^2}{8m_b^2 X_b^2} \right) \ll M_S^2. \quad (35)$$

This scenario is termed maximal mixing since

$$\sin 2\tilde{\theta}_b \sim 1 - \frac{(\tilde{m}_L^2 - \tilde{m}_R^2)^2 (1 + \Delta_b)^2}{8m_b^2 X_b^2}. \quad (36)$$

We expand the contributions of the exact one-loop SQCD calculation given in Appendix B in powers of $1/M_S$, keeping terms to $\mathcal{O}\left(\frac{M_{EW}^2}{M_S^2}\right)$ and assuming $M_S \sim M_{\tilde{g}} \sim \mu \sim A_b \sim \tilde{m}_L \sim \tilde{m}_R \gg M_W, M_Z, M_h \sim M_{EW}$. In the expansions, we assume the large $\tan\beta$ limit and take $m_b \tan\beta \sim \mathcal{O}(M_{EW})$. This expansion has been studied in detail for the decay $h \rightarrow b\bar{b}$, with particular emphasis on the decoupling properties of the results as M_S and $M_{\tilde{g}} \rightarrow \infty$ [28]. The SQCD contributions to the decay, $h \rightarrow b\bar{b}$, extracted from our results are in agreement with those of Refs. [28, 42]

The final result for maximal mixing, summing all contributions, is,

$$A_s \equiv -g_s T^A g_{bbh} M_s^\mu \left\{ 1 + \frac{\alpha_s(\mu_R)}{4\pi} X_i^s \right\} \\ = -g_s T^A g_{bbh} M_s^\mu \left\{ 1 + \left(\frac{\delta g_{bbh}}{g_{bbh}} \right)_{max} + \frac{\alpha_s(\mu_R)}{4\pi} \frac{s}{M_S^2} \delta\kappa_{max} \right\} \\ A_t \equiv -g_s T^A g_{bbh} M_s^\mu \left\{ 1 + \frac{\alpha_s(\mu_R)}{4\pi} X_i^t \right\} \\ = -g_s T^A g_{bbh} M_t^\mu \left\{ 1 + \left(\frac{\delta g_{bbh}}{g_{bbh}} \right)_{max} \right\} \\ A_1 \equiv -g_s T^A g_{bbh} M_s^\mu \left\{ 1 + \frac{\alpha_s(\mu_R)}{4\pi} X_i^1 \right\} \\ = -g_s T^A g_{bbh} M_1^\mu \left(-\frac{\alpha_s(\mu_R)u}{2\pi M_S^2} \right) \delta\kappa_{max}. \quad (37)$$

The contribution which is a rescaling of the $b\bar{b}h$ vertex is,

$$\left(\frac{\delta g_{bbh}}{g_{bbh}}\right)_{max} = \left(\frac{\delta g_{bbh}}{g_{bbh}}\right)_{max}^{(1)} + \left(\frac{\delta g_{bbh}}{g_{bbh}}\right)_{max}^{(2)}, \quad (38)$$

where the leading order term in M_{EW}/M_S is $\mathcal{O}(1)$,

$$\left(\frac{\delta g_{bbh}}{g_{bbh}}\right)_{max}^{(1)} = \frac{\alpha_s(\mu_R)}{3\pi} \frac{M_{\tilde{g}}(X_b - Y_b)}{M_S^2} f_1(R), \quad (39)$$

with $Y_b \equiv A_b + \mu \cot \alpha$ and $R \equiv M_{\tilde{g}}/M_S$. Eq. 39 only decouples for large M_S if the additional limit $M_A \rightarrow \infty$ is also taken[23, 28]. In this limit,

$$X_b - Y_b \rightarrow \frac{2\mu M_Z^2}{M_A^2} \tan \beta \cos 2\beta + \mathcal{O}\left(\frac{M_{EW}^4}{M_A^4}\right). \quad (40)$$

The subleading terms of $\mathcal{O}(M_{EW}^2/M_S^2)$ are,⁸

$$\begin{aligned} \left(\frac{\delta g_{bbh}}{g_{bbh}}\right)_{max}^{(2)} &= \frac{\alpha_s(\mu_R)}{3\pi} \left\{ -\frac{M_{\tilde{g}} Y_b}{M_S^2} \left[\frac{M_h^2}{12M_S^2} f_3^{-1}(R) + \frac{X_b^2 m_b^2}{2(1+\Delta_b)^2 M_S^4} f_3(R) \right] \right. \\ &\quad - \frac{m_b^2 X_b Y_b}{2(1+\Delta_b)^2 M_S^4} f_3^{-1}(R) \\ &\quad \left. + \frac{M_Z^2}{3M_S^2} \frac{c_\beta s_{\alpha+\beta}}{s_\alpha} I_3^b \left[3f_1(R) + \left(\frac{2M_{\tilde{g}} X_b}{M_S^2} - 1 \right) f_2(R) \right] \right\} \end{aligned} \quad (41)$$

The functions $f_i(R)$ are defined in Appendix C.

The $\frac{s}{M_S^2}, \frac{u}{M_S^2}$ terms in Eq. 37 are not a rescaling of the lowest order vertex and cannot be obtained from the effective Lagrangian. We find,

$$\delta\kappa_{max} = \frac{1}{4} \left[f_3(R) + \frac{1}{9} f_3^{-1}(R) \right] - R \frac{Y_b}{2M_S} \left[f_2'(R) + \frac{1}{9} \hat{f}_2(R) \right]. \quad (42)$$

The $\delta\kappa_{max}$ term is $\mathcal{O}(1)$ in M_{EW}/M_S and has its largest values for small R and large ratios of Y_b/M_S , as can be seen in Fig. 2. Large effects can be obtained for $Y_b/M_S \sim 10$ and $M_{\tilde{g}} \ll M_S$. However, the parameters must be carefully tuned so that $A_b/M_S \lesssim 1$ in order not to break color[45].

The amplitude squared, summing over final state spins and colors and averaging over initial state spins and colors, including one-loop SQCD corrections is

$$|\overline{\mathcal{A}}|_{max}^2 = -\frac{2\pi\alpha_s(\mu_R)}{3} g_{bbh}^2 \left[\left(\frac{u^2 + M_h^4}{st} \right) \left[1 + 2 \left(\frac{\delta g_{bbh}}{g_{bbh}} \right)_{max} \right] + \frac{\alpha_s(\mu_R)}{2\pi} \frac{M_h^2}{M_S^2} \delta\kappa_{max} \right]. \quad (43)$$

⁸ We use the shorthand, $c_\beta = \cos \beta$, $s_{\alpha+\beta} = \sin(\alpha + \beta)$, etc.

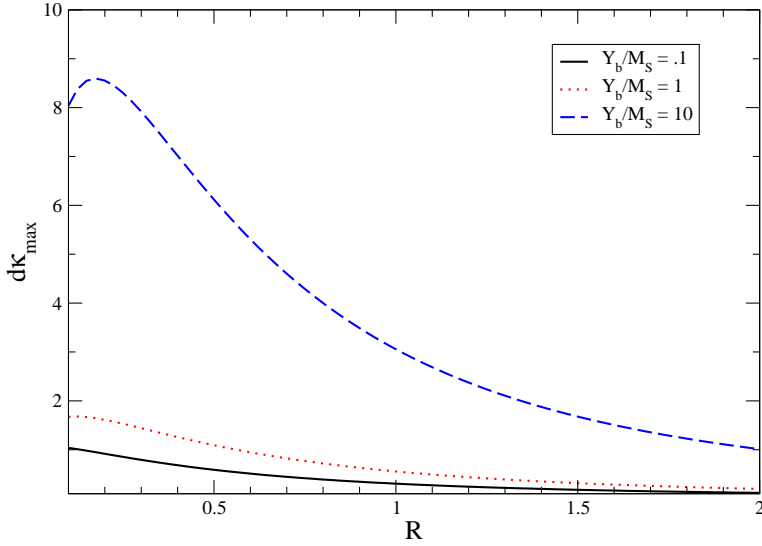


FIG. 2: Contribution of $\delta\kappa_{max}$ defined in Eq. 42 as a function of $R = M_{\tilde{g}}/M_S$.

Note that in the cross section, the $\delta\kappa_{max}$ term is not enhanced by a power of s and gives a contribution of $\mathcal{O}\left(\frac{M_{EW}^2}{M_S^2}\right)$.

Expanding Δ_b in the maximal mixing limit,

$$\Delta_b \rightarrow -\frac{\alpha_s(\mu_S)}{3\pi} \frac{M_{\tilde{g}}\mu}{M_S^2} \tan\beta f_1(R) + \mathcal{O}\left(\frac{M_{EW}^4}{M_S^4}\right). \quad (44)$$

By comparison with Eq. 14,

$$\begin{aligned} |\overline{\mathcal{A}}|_{max}^2 &= -\frac{2\pi\alpha_s(\mu_R)}{3} (g_{bbh}^{\Delta_b})^2 \left\{ \left(\frac{u^2 + M_h^4}{st} \right) \left[1 + 2 \left(\frac{\delta g_{bbh}}{g_{bbh}} \right)_{max}^{(2)} \right] \right. \\ &\quad \left. + \frac{\alpha_s(\mu_R)}{2\pi} \frac{M_h^2}{M_S^2} \delta\kappa_{max} \right\} + \mathcal{O}\left(\left[\frac{M_{EW}}{M_S}\right]^4, \alpha_s^3\right). \end{aligned} \quad (45)$$

Note that the mis-match in the arguments of α_s in Eqs. 44 and 45 is higher order in α_s than the terms considered here. The $(\delta g_{bbh}/g_{bbh})_{max}^{(2)}$ and $\delta\kappa_{max}$ terms both correspond to contributions which are not present in the effective Lagrangian approach. These terms are, however, suppressed by powers of M_{EW}^2/M_S^2 and the non-decoupling effects discussed in Refs. [28] and [27] are completely contained in the $g_{bbh}^{\Delta_b}$ term.

B. Minimal Mixing in the b Squark Sector

The minimal mixing scenario is characterized by a mass splitting between the b squarks which is of order the b squark mass, $|M_{\tilde{b}_1}^2 - M_{\tilde{b}_2}^2| \sim M_S^2$. In this case,

$$|\tilde{m}_L^2 - \tilde{m}_R^2| \gg \frac{m_b |X_b|}{(1 + \Delta_b)}, \quad (46)$$

and the mixing angle in the b squark sector is close to zero,

$$\cos 2\tilde{\theta}_b \sim 1 - \frac{2m_b^2 X_b^2}{(M_{\tilde{b}_1}^2 - M_{\tilde{b}_2}^2)^2} \left(\frac{1}{1 + \Delta_b} \right)^2. \quad (47)$$

The non-zero subamplitudes are

$$\begin{aligned} A_s &= -g_s T^A g_{bbh} M_s^\mu \left\{ 1 + \left(\frac{\delta g_{bbh}}{g_{bbh}} \right)_{min} + \frac{\alpha_s(\mu_R)}{4\pi} \frac{s}{\tilde{M}_g^2} \delta\kappa_{min} \right\} \\ A_t &= -g_s T^A g_{bbh} M_t^\mu \left\{ 1 + \left(\frac{\delta g_{bbh}}{g_{bbh}} \right)_{min} \right\} \\ A_1 &= -g_s T^A g_{bbh} M_1^\mu \left(-\frac{\alpha_s(\mu_R)u}{2\pi \tilde{M}_g^2} \right) \delta\kappa_{min}. \end{aligned} \quad (48)$$

Expanding the exact one-loop results of Appendix B in the minimal mixing scenario,

$$\delta\kappa_{min} = \frac{1}{8} \sum_{i=1}^2 \left(R_i^2 \left[\frac{1}{9} f_3^{-1}(R_i) + f_3(R_i) \right] \right) + \frac{Y_b}{\tilde{M}_g} \frac{R_1^2 R_2^2}{R_2^2 - R_1^2} \left(3h_1(R_1, R_2, 1) + \frac{8}{3} h_1(R_1, R_2, 2) \right), \quad (49)$$

where $R_i = M_{\tilde{g}}/M_{\tilde{b}_i}$ and the functions $f_i(R_i)$ and $h_i(R_1, R_2, n)$ are defined in Appendix C. The $\delta\kappa_{min}$ function is shown in Fig. 3. For large values of $Y_b/M_{\tilde{g}}$ it can be significantly larger than 1.

As in the previous section, the spin and color averaged amplitude-squared is,

$$|\overline{A}|_{min}^2 = -\frac{2\alpha_s(\mu_R)\pi}{3} (g_{bbh}^2) \left\{ \frac{(M_h^4 + u^2)}{st} \left[1 + 2 \left(\frac{\delta g_{bbh}}{g_{bbh}} \right)_{min} \right] + \frac{\alpha_s(\mu_R)}{2\pi} \delta\kappa_{min} \frac{M_h^2}{\tilde{M}_g^2} \right\}, \quad (50)$$

with,

$$\left(\frac{\delta g_{bbh}}{g_{bbh}} \right)_{min} = \left(\frac{\delta g_{bbh}}{g_{bbh}} \right)_{min}^{(1)} + \left(\frac{\delta g_{bbh}}{g_{bbh}} \right)_{min}^{(2)}. \quad (51)$$

The leading order term in M_{EW}/M_S is $\mathcal{O}(1)$,

$$\left(\frac{\delta g_{bbh}}{g_{bbh}} \right)_{min}^{(1)} = \frac{2\alpha_s(\mu_R)}{3\pi} \frac{(X_b - Y_b)}{M_{\tilde{g}}} \frac{R_1^2 R_2^2}{R_1^2 - R_2^2} h_1(R_1, R_2, 0). \quad (52)$$

$$R_2 = 2 R_1$$

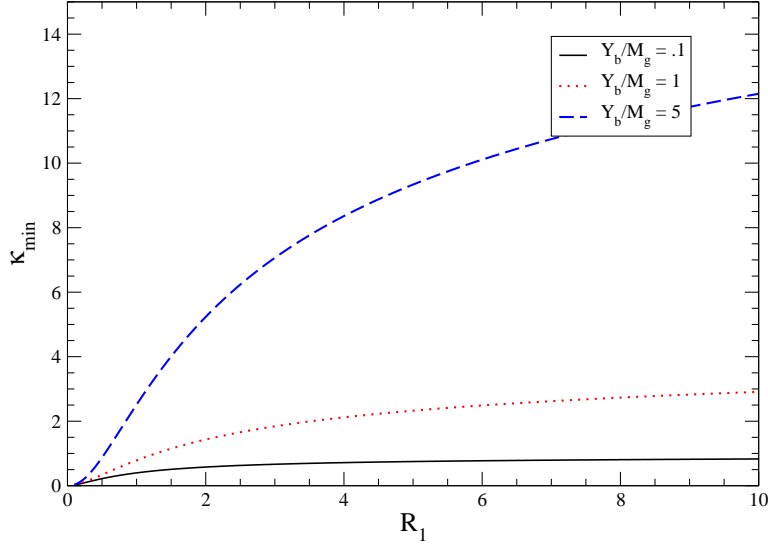


FIG. 3: Contribution of $\delta\kappa_{min}$ defined in Eq. 49 as a function of $R_i = M_{\bar{g}}/M_{\bar{b}_i}$.

The subleading terms are $\mathcal{O}\left(\frac{M_{EW}^2}{M_S^2}\right)$,

$$\begin{aligned}
\left(\frac{\delta g_{bbh}}{g_{bbh}}\right)_{min}^{(2)} &= \frac{\alpha_s}{4\pi} \left\{ -\frac{8M_{\bar{g}}Y_b}{3\Delta M_{\bar{b}_{12}}^2} \left[\frac{h_2(R_1, R_2) M_h^2}{\Delta M_{\bar{b}_{12}}^2} \right. \right. \\
&+ \left. \frac{m_b^2 X_b^2}{(\Delta M_{\bar{b}_{12}}^2)^2 (1 + \Delta_b)^2} \left\{ 2\mathcal{S}\left(\frac{f_1(R)}{M_b^2}\right) + \frac{h_1(R_1, R_2, 0)}{\Delta M_{\bar{b}_{12}}^2} \right\} \right] \\
&+ \frac{4c_\beta s_{\alpha+\beta}}{3s_\alpha} I_3^b M_Z^2 \left[\mathcal{S}\left(\frac{3f_1(R) - f_2(R)}{3M_b^2}\right) - \frac{2M_{\bar{g}}X_b}{\Delta M_{\bar{b}_{12}}^2} \mathcal{A}\left(\frac{f_1(R)}{M_b^2}\right) \right] \\
&+ \frac{4c_\beta s_{\alpha+\beta}}{3s_\alpha} (I_3^b - 2Q^b s_W^2) M_Z^2 \left[\mathcal{A}\left(\frac{3f_1(R) - f_2(R)}{3M_b^2}\right) \right. \\
&- \left. \frac{2M_{\bar{g}}X_b}{\Delta M_{\bar{b}_{12}}^2} \left\{ \mathcal{S}\left(\frac{f_1(R)}{M_b^2}\right) + \frac{h_1(R_1, R_2, 0)}{\Delta M_{\bar{b}_{12}}^2} \right\} \right] \\
&+ \left. \frac{8}{3} \frac{m_b^2 X_b Y_b}{\Delta M_{\bar{b}_{12}}^2 (1 + \Delta_b)^2} \mathcal{A}\left(\frac{3f_1(R) - f_2(R)}{3M_b^2}\right) \right\}. \tag{53}
\end{aligned}$$

The symmetric and anti-symmetric functions are defined,

$$\begin{aligned}
\mathcal{S}(f(R, M_{\bar{b}})) &\equiv \frac{1}{2} \left[f(R_1, M_{\bar{b}_1}) + f(R_2, M_{\bar{b}_2}) \right] \\
\mathcal{A}(f(R, M_{\bar{b}})) &\equiv \frac{1}{2} \left[f(R_1, M_{\bar{b}_1}) - f(R_2, M_{\bar{b}_2}) \right] \tag{54}
\end{aligned}$$

and $\Delta M_{\tilde{b}_{12}}^2 \equiv M_{\tilde{b}_1}^2 - M_{\tilde{b}_2}^2$. The remaining functions are defined in Appendix C.

By expanding Δ_b in the minimal mixing limit, we find the analogous result to that of the maximal mixing case,

$$|\overline{A}|_{min}^2 = -\frac{2\alpha_s\pi}{3}(g_{bb\tilde{h}}^{\Delta_b})^2 \left\{ \frac{(M_h^4 + u^2)}{st} \left[1 + 2 \left(\frac{\delta g_{bb\tilde{h}}}{g_{bb\tilde{h}}} \right)_{min}^{(2)} \right] + \frac{\alpha_s}{2\pi} \delta\kappa_{min} \frac{M_h^2}{M_{\tilde{g}}^2} \right\} + \mathcal{O} \left(\left[\frac{M_{EW}}{M_S} \right]^4, \alpha_s^3 \right). \quad (55)$$

The contributions which are not contained in σ_{IBA} are again found to be suppressed by $\mathcal{O} \left(\left[\frac{M_{EW}}{M_S} \right]^2 \right)$.

IV. NUMERICAL RESULTS

We present results for $pp \rightarrow b(\bar{b})h$ at $\sqrt{s} = 7 \text{ TeV}$ with $p_{Tb} > 20 \text{ GeV}$ and $|\eta_b| < 2.0$. We use FeynHiggs to generate M_h and $\sin\alpha_{eff}$ and then iteratively solve for the b squark masses and Δ_b from Eqs. 12 and 19. We evaluate the 2-loop \overline{MS} b mass at $\mu_R = M_h/2$, which we also take to be the renormalization and factorization scales⁹. Finally, Figs 4, 5, 6, and 7 use the CTEQ6m NLO parton distribution functions[46]. Figs. 4, 5 and 6 show the percentage deviation of the complete one-loop SQCD calculation from the Improved Born Approximation of Eq. 16 for $\tan\beta = 40$ and $\tan\beta = 20$ and representative values of the MSSM parameters¹⁰. In both extremes of b squark mixing, the Improved Born Approximation approximation is within a few percent of the complete one-loop SQCD calculation and so is a reliable prediction for the rate. This is true for both large and small M_A . In addition, the large M_S expansion accurately reproduces the full SQCD one-loop result to within a few percent. These results are expected from the expansions of Eqs. 45 and 55, since the terms which differ between the Improved Born Approximation and the one-loop calculation are suppressed in the large M_S limit.

Fig. 7 compares the total SQCD rate for maximal and minimal mixing, which bracket the allowed mixing possibilities. For large M_S , the effect of the mixing is quite small, while for $M_S \sim 800 \text{ GeV}$, the mixing effects are at most a few fb . The accuracy of the Improved Born Approximation as a function of m_R is shown in Fig. 8 for fixed M_A, μ , and m_L . As

⁹ Δ_b is evaluated using $\alpha_s(M_S)$.

¹⁰ Figs. 4, 5 and 6 do not include the pure QCD NLO corrections[17].

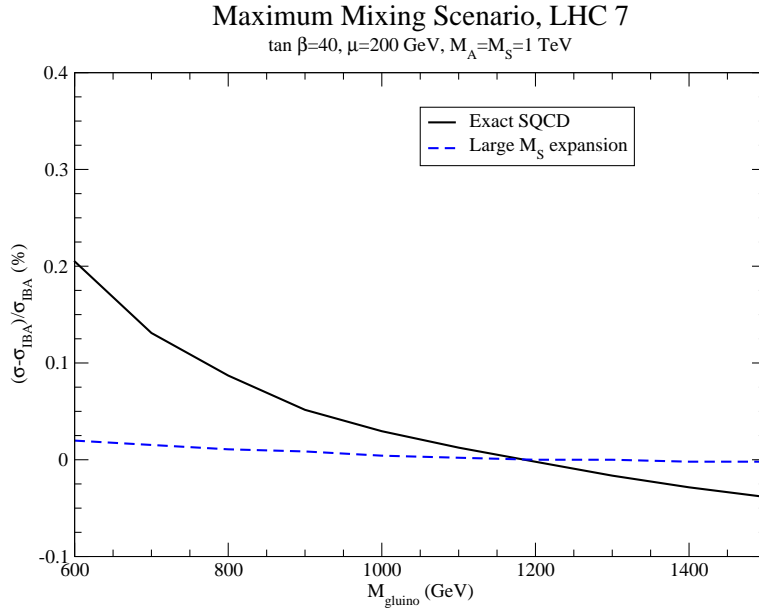


FIG. 4: Percentage difference between the Improved Born Approximation and the exact one-loop SQCD calculation of $pp \rightarrow bh$ for maximal mixing in the b -squark sector at $\sqrt{s} = 7 \text{ TeV}$, $\tan \beta = 40$, and $M_A = 1 \text{ TeV}$.

m_R is increased, the effects become very tiny. Even for light gluino masses, the Improved Born Approximation reproduces the exact SQCD result to within a few percent.

In Fig. 9, we show the scale dependence for the total rate, including NLO QCD and SQCD corrections (dotted lines) for a representative set of MSSM parameters at $\sqrt{s} = 7 \text{ TeV}$. The NLO scale dependence is quite small when $\mu_R = \mu_F \sim M_h$. However, there is a roughly $\sim 5\%$ difference between the predictions found using the CTEQ6m PDFs and the MSTW2008 NLO PDFs[47]. In Fig. 10, we show the scale dependence for small μ_F (as preferred by [16]), and see that it is significantly larger than in Fig. 9. This is consistent with the results of [19, 29].

V. CONCLUSION

Our major results are the analytic expressions for the SQCD corrections to b Higgs associated production in the minimal (Eqs. 41, 42 and 45) and maximal (Eqs. 49, 53 and 55) b squark mixing scenarios for large $\tan \beta$ and squark masses, M_S . These results

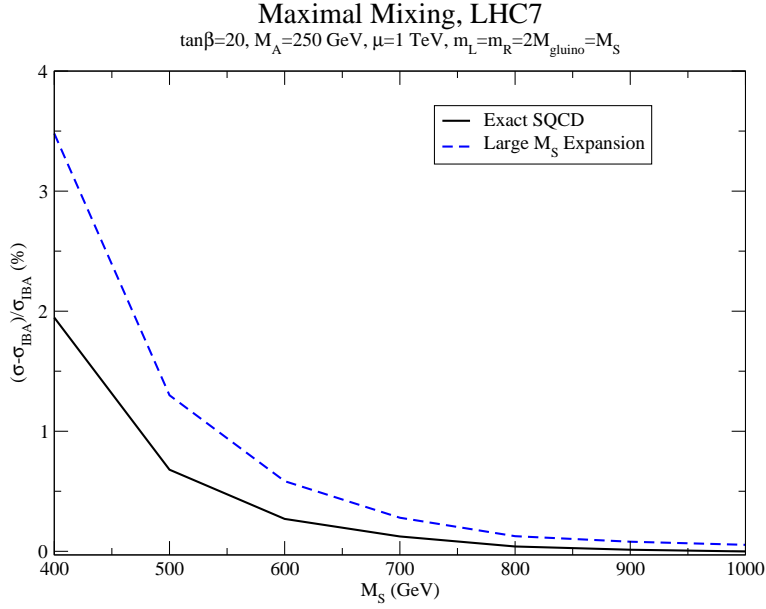


FIG. 5: Percentage difference between the Improved Born Approximation and the exact one-loop SQCD calculation of $pp \rightarrow bh$ for maximal mixing in the b -squark sector at $\sqrt{s} = 7 \text{ TeV}$, $\tan \beta = 20$, and $M_A = 250 \text{ GeV}$.

clearly demonstrate that deviations from the Δ_b approximation are suppressed by powers of (M_{EW}/M_S) in the large $\tan \beta$ region. The Δ_b approximation hence yields an accurate prediction in the 5 flavor number scheme for the cross section for squark and gluino masses at the TeV scale. As a by-product of our calculation, we update the predictions for b Higgs production at $\sqrt{s} = 7 \text{ TeV}$.

Acknowledgements

S. Dawson and P.Jaiswal are supported by the United States Department of Energy under Grant DE-AC02-98CH10886.

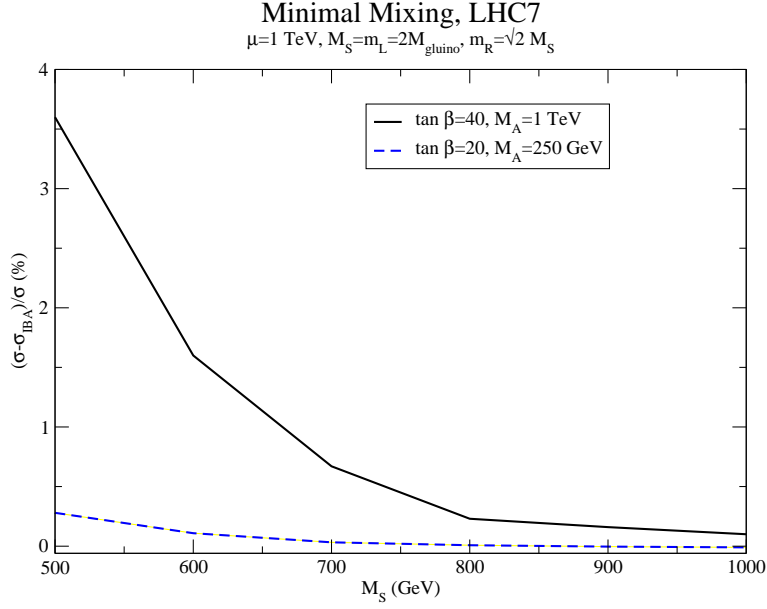


FIG. 6: Percentage difference between the Improved Born Approximation and the exact one-loop SQCD calculation for $pp \rightarrow bh$ for minimal mixing in the b squark sector at $\sqrt{s} = 7 \text{ TeV}$.

Appendix A: Passarino-Veltman Functions

The scalar integrals are defined as:

$$\begin{aligned}
 \frac{i}{16\pi^2} A_0(M_0^2) &= \int \frac{d^n k}{(2\pi)^n} \frac{1}{N_0}, \\
 \frac{i}{16\pi^2} B_0(p_1^2; M_0^2, M_1^2) &= \int \frac{d^n k}{(2\pi)^n} \frac{1}{N_0 N_1}, \\
 \frac{i}{16\pi^2} C_0(p_1^2, p_2^2, (p_1 + p_2)^2; M_0^2, M_1^2, M_2^2) &= \int \frac{d^n k}{(2\pi)^n} \frac{1}{N_0 N_1 N_2}, \\
 \frac{i}{16\pi^2} D_0(p_1^2, p_2^2, p_3^2, p_4^2, (p_1 + p_2)^2, (p_2 + p_3)^2; M_0^2, M_1^2, M_2^2, M_3^2) \\
 &= \int \frac{d^n k}{(2\pi)^n} \frac{1}{N_0 N_1 N_2 N_3},
 \end{aligned} \tag{56}$$

where,

$$\begin{aligned}
 N_0 &= k^2 - M_0^2 \\
 N_1 &= (k + p_1)^2 - M_1^2 \\
 N_2 &= (k + p_1 + p_2)^2 - M_2^2 \\
 N_3 &= (k + p_1 + p_2 + p_3)^2 - M_3^2.
 \end{aligned} \tag{57}$$

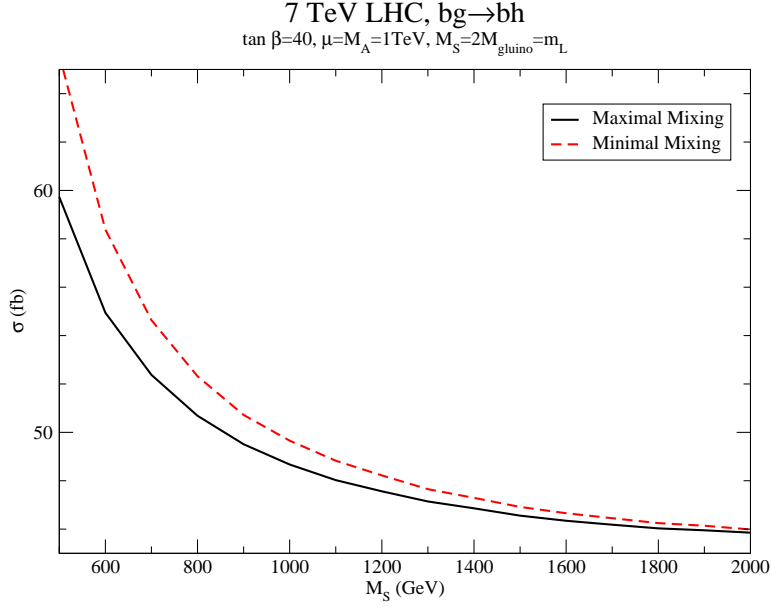


FIG. 7: Comparison between the exact one-loop SQCD calculation for $pp \rightarrow bh$ for minimal and maximal mixing in the b squark sector at $\sqrt{s} = 7 \text{ TeV}$ and $\tan \beta = 40$. The minimal mixing curve has $m_R = \sqrt{2}M_S$ and $\tilde{\theta}_b \sim 0$, while the maximal mixing curve has $m_R = M_S$ and $\tilde{\theta}_b \sim \frac{\pi}{4}$.

The tensor integrals encountered are expanded in terms of the external momenta p_i and the metric tensor $g^{\mu\nu}$. For the two-point function we write:

$$\begin{aligned} \frac{i}{16\pi^2} B^\mu(p_1^2; M_0^2, M_1^2) &= \int \frac{d^n k}{(2\pi)^n} \frac{k^\mu}{N_0 N_1} \\ &\equiv \frac{i}{16\pi^2} p_1^\mu B_1(p_1^2, M_0^2, M_1^2), \end{aligned} \quad (58)$$

while for the three-point functions we have both rank-one and rank-two tensor integrals which we expand as:

$$\begin{aligned} C^\mu(p_1^2, p_2^2, (p_1 + p_2)^2; M_0^2, M_1^2, M_2^2) &= p_1^\mu C_{11} + p_2^\mu C_{12}, \\ C^{\mu\nu}(p_1^2, p_2^2, (p_1 + p_2)^2; M_0^2, M_1^2, M_2^2) &= p_1^\mu p_1^\nu C_{21} + p_2^\mu p_2^\nu C_{22} \\ &\quad + (p_1^\mu p_2^\nu + p_1^\nu p_2^\mu) C_{23} + g^{\mu\nu} C_{24}, \end{aligned} \quad (59)$$

where:

$$\frac{i}{16\pi^2} C^\mu(C^{\mu\nu})(p_1^2, p_2^2, (p_1 + p_2)^2; M_0^2, M_1^2, M_2^2) \equiv \int \frac{d^n k}{(2\pi)^n} \frac{k^\mu(k^\mu k^\nu)}{N_0 N_1 N_2} \quad (60)$$

Finally, for the box diagrams, we encounter rank-one and rank-two tensor integrals which

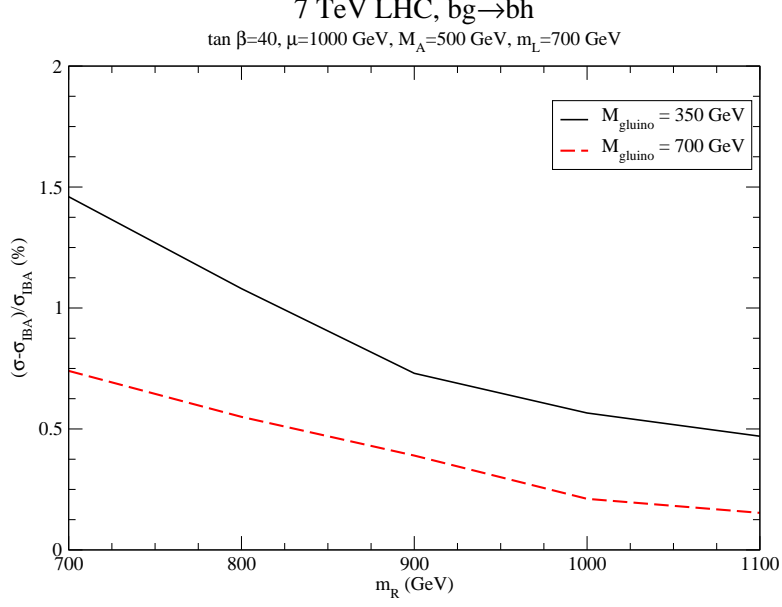


FIG. 8: Percentage difference between the Improved Born Approximation and the exact one-loop SQCD calculation for $pp \rightarrow bh$ as a function of m_R at $\sqrt{s} = 7 \text{ TeV}$ and $\tan \beta = 40$.

are written in terms of the Passarino-Veltmann coefficients as:

$$\begin{aligned} \frac{i}{16\pi^2} D^\mu(p_1^2, p_2^2, p_3^2, p_4^2, (p_1 + p_2)^2, (p_2 + p_3)^2; M_0^2, M_1^2, M_2^2) &\equiv \int \frac{d^n k}{(2\pi)^n} \frac{k^\mu}{N_0 N_1 N_2 N_3} \\ &= \frac{i}{16\pi^2} \left\{ p_1^\mu D_{11} + p_2^\mu D_{12} + p_3^\mu D_{13} \right\}. \end{aligned} \quad (61)$$

$$\begin{aligned} \frac{i}{16\pi^2} D^{\mu\nu}(p_1^2, p_2^2, p_3^2, p_4^2, (p_1 + p_2)^2, (p_2 + p_3)^2; M_0^2, M_1^2, M_2^2) &\equiv \int \frac{d^n k}{(2\pi)^n} \frac{k^\mu k^\nu}{N_0 N_1 N_2 N_3} \\ &= \frac{i}{16\pi^2} \left\{ g^{\mu\nu} D_{00} + \text{tensor structures not needed here} \right\}. \end{aligned} \quad (62)$$

Appendix B: One-Loop Results

In this appendix we give the non-zero contributions of the individual diagrams in terms of the basis functions of Eq. 20 and the decompositions of Eq. 22. The contributions proportional to $m_b \tan \beta$ are new and were not included in the results of Ref.[23]. Although we specialize to the case of the lightest Higgs boson, h , our results are easily generalized to the heavier neutral Higgs boson, H , and so the Feynman diagrams in this appendix are shown for $\phi_i = h, H$.

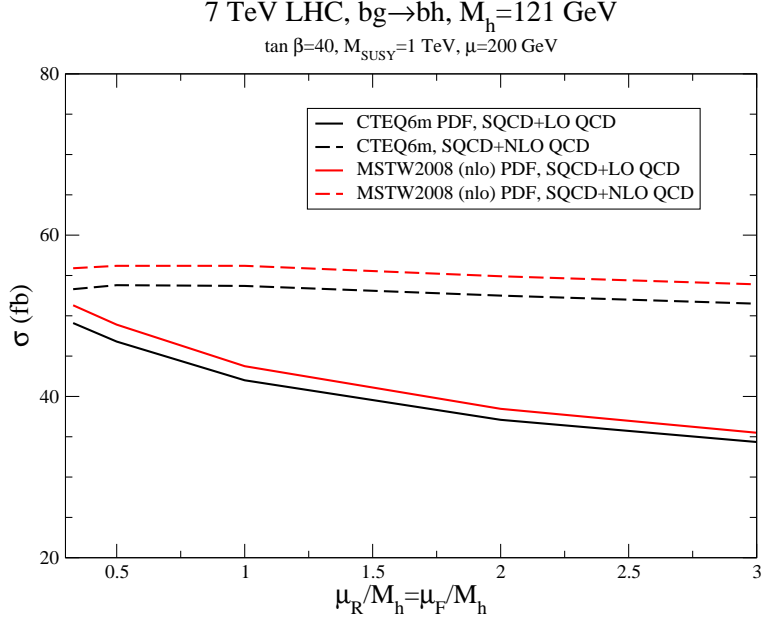


FIG. 9: Total cross section for $pp \rightarrow b(\bar{b})h$ production including NLO QCD and SQCD corrections (dotted lines) as a function of renormalization/factorization scale using CTEQ6m (black) and MSTW2008 NLO (red) PDFs. We take $M_{\tilde{g}} = 1$ TeV and the remaining MSSM parameters as in Fig. 4.

The self-energy diagrams of Fig. 11:

$$\begin{aligned}
 X_{S_1}^{(t)} &= \frac{4}{3} \sum_{i=1}^2 \left\{ B_1 - (-1)^i \frac{2m_b M_{\tilde{g}} s_{2\tilde{b}}}{t} B_0 \right\} (M_{\tilde{b}_i}^2) \\
 X_{S_1}^{(2)} &= -\frac{4}{3} \sum_{i=1}^2 (-1)^i \frac{m_b M_{\tilde{g}} s_{2\tilde{b}}}{t} B_0 (M_{\tilde{b}_i}^2)
 \end{aligned} \tag{63}$$

where we have used the shorthand notation for the arguments of Passarino-Veltman functions, $B_{0,1}(M_{\tilde{b}_i}^2) \equiv B_{0,1}(t; M_{\tilde{g}}^2, M_{\tilde{b}_i}^2)$.

$$\begin{aligned}
 X_{S_2}^{(s)} &= \frac{4}{3} \sum_{i=1}^2 \left\{ B_1 - (-1)^i \frac{2m_b M_{\tilde{g}} s_{2\tilde{b}}}{s} B_0 \right\} (M_{\tilde{b}_i}^2) \\
 X_{S_2}^{(2)} &= -\frac{4}{3} \sum_{i=1}^2 (-1)^i \frac{m_b M_{\tilde{g}} s_{2\tilde{b}}}{s} B_0 (M_{\tilde{b}_i}^2)
 \end{aligned} \tag{64}$$

and $B_{0,1}(M_{\tilde{b}_i}^2) \equiv B_{0,1}(s; M_{\tilde{g}}^2, M_{\tilde{b}_i}^2)$

The vertex functions of Fig. 12:

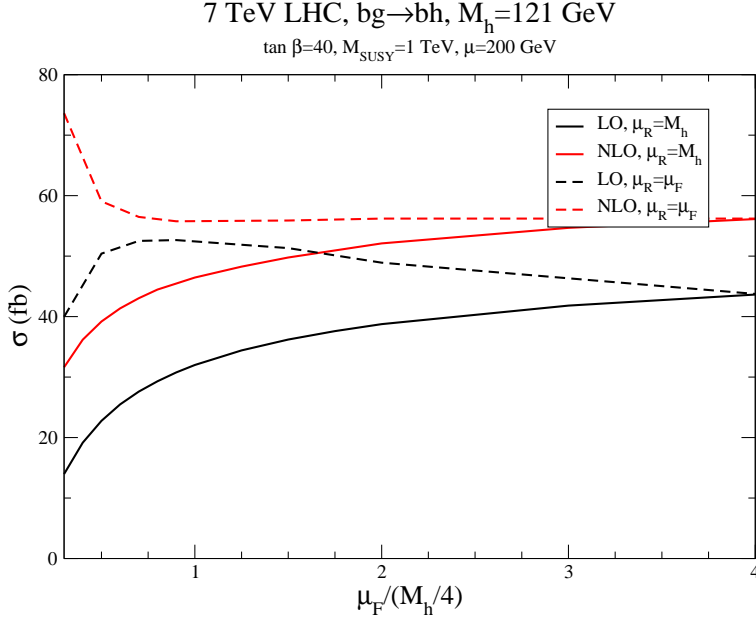


FIG. 10: Total cross section for $pp \rightarrow b(\bar{b})h$ production including NLO QCD and SQCD corrections as a function of the factorization scale using MSTW2008 NLO PDFs. We take $M_{\tilde{g}} = 1$ TeV and the remaining MSSM parameters as in Fig. 4.

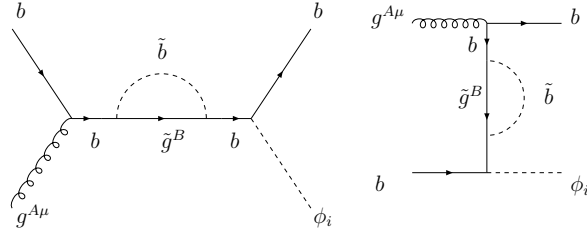


FIG. 11: Self-energy diagrams, S_1 and S_2 .

Diagram V_1 :

$$\begin{aligned}
 X_{V_1}^{(s)} &= \frac{s}{6} \sum_{i=1}^2 \left\{ C_{12} + C_{23} - (-1)^i \frac{2m_b M_{\tilde{g}} s_{2\tilde{b}}}{t} (C_0 + C_{11}) \right\} (M_{b_i}^2) \\
 X_{V_1}^{(t)} &= -\frac{1}{6} \sum_{i=1}^2 \left\{ t (C_{12} + C_{23}) + 2C_{24} - (-1)^i 2m_b M_{\tilde{g}} s_{2\tilde{b}} (C_0 + C_{11}) \right\} (M_{b_i}^2) \\
 X_{V_1}^{(1)} &= -\frac{u}{3} \sum_{i=1}^2 \left\{ C_{12} + C_{23} - (-1)^i \frac{2m_b M_{\tilde{g}} s_{2\tilde{b}}}{t} (C_0 + C_{11}) \right\} (M_{b_i}^2) \\
 X_{V_1}^{(3)} &= -\frac{1}{3} \sum_i (-1)^i m_b M_{\tilde{g}} s_{2\tilde{b}} (C_0 + C_{11}) (M_{b_i}^2)
 \end{aligned} \tag{65}$$

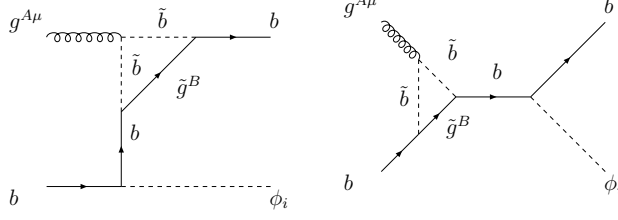


FIG. 12: Virtual diagrams, V_1 and V_2 .

where $C_{0,11,12,23,24} \left(M_{\tilde{b}_i}^2 \right) \equiv C_{0,11,12,23,24} \left(0, 0, t; M_{\tilde{g}}^2, M_{\tilde{b}_i}^2, M_{\tilde{b}_i}^2 \right)$.

Diagram V_2 :

$$\begin{aligned}
 X_{V_2}^{(s)} &= -\frac{1}{3} \sum_{i=1}^2 C_{24} \left(M_{\tilde{b}_i}^2 \right) \\
 X_{V_2}^{(1)} &= -\frac{u}{3} \sum_{i=1}^2 \left\{ C_{12} + C_{23} - (-1)^i \frac{2m_b M_{\tilde{g}} s_{2\tilde{b}}}{s} (C_0 + C_{11}) \right\} \left(M_{\tilde{b}_i}^2 \right) \\
 X_{V_2}^{(4)} &= \frac{1}{3} \sum_i (-1)^i m_b M_{\tilde{g}} s_{2\tilde{b}} (C_0 + C_{11}) \left(M_{\tilde{b}_i}^2 \right)
 \end{aligned} \tag{66}$$

where $C_{0,11,12,23,24} \left(M_{\tilde{b}_i}^2 \right) \equiv C_{0,11,12,23,24} \left(0, 0, s; M_{\tilde{g}}^2, M_{\tilde{b}_i}^2, M_{\tilde{b}_i}^2 \right)$.

The vertex functions of Fig. 13:

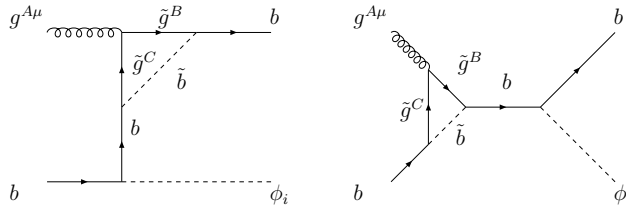


FIG. 13: Virtual diagrams, V_3 and V_4 .

Diagram V_3 :

$$\begin{aligned}
X_{V_3}^{(s)} &= \frac{3s}{2} \sum_{i=1}^2 \left\{ C_{12} + C_{23} - (-1)^i \frac{2m_b M_{\tilde{g}} s_{2\tilde{b}}}{t} (C_0 + C_{12}) \right\} \left(M_{\tilde{b}_i}^2 \right) \\
X_{V_3}^{(t)} &= -\frac{3}{2} \sum_{i=1}^2 \left\{ M_{\tilde{g}}^2 C_0 - 2(1-\epsilon) C_{24} - (-1)^i 2m_b M_{\tilde{g}} s_{2\tilde{b}} C_{12} \right\} \left(M_{\tilde{b}_i}^2 \right) \\
X_{V_3}^{(1)} &= -3u \sum_{i=1}^2 \left\{ C_{12} + C_{23} - (-1)^i \frac{2m_b M_{\tilde{g}} s_{2\tilde{b}}}{t} (C_0 + C_{12}) \right\} \left(M_{\tilde{b}_i}^2 \right) \\
X_{V_3}^{(2)} &= -\frac{3}{2} \sum_{i=1}^2 (-1)^i m_b M_{\tilde{g}} s_{2\tilde{b}} C_0 \left(M_{\tilde{b}_i}^2 \right) \\
X_{V_3}^{(3)} &= -3 \sum_{i=1}^2 (-1)^i m_b M_{\tilde{g}} s_{2\tilde{b}} \{C_0 + C_{12}\} \left(M_{\tilde{b}_i}^2 \right) \tag{67}
\end{aligned}$$

where $C_{0,11,12,23,24} \left(M_{\tilde{b}_i}^2 \right) \equiv C_{0,11,12,23,24} \left(0, 0, t; M_{\tilde{g}}^2, M_{\tilde{g}}^2, M_{\tilde{b}_i}^2 \right)$.

Diagram V_4 :

$$\begin{aligned}
X_{V_4}^{(s)} &= -\frac{3}{2} \sum_{i=1}^2 \left\{ M_{\tilde{g}}^2 C_0 - 2(1-\epsilon) C_{24} - s(C_{12} + C_{23}) + (-1)^i 2m_b M_{\tilde{g}} s_{2\tilde{b}} C_0 \right\} \left(M_{\tilde{b}_i}^2 \right) \\
X_{V_4}^{(1)} &= -3u \sum_{i=1}^2 \left\{ C_{12} + C_{23} - (-1)^i \frac{2m_b M_{\tilde{g}} s_{2\tilde{b}}}{s} (C_0 + C_{12}) \right\} \left(M_{\tilde{b}_i}^2 \right) \\
X_{V_4}^{(2)} &= -\frac{3}{2} \sum_{i=1}^2 (-1)^i m_b M_{\tilde{g}} s_{2\tilde{b}} C_0 \left(M_{\tilde{b}_i}^2 \right) \\
X_{V_4}^{(4)} &= 3 \sum_{i=1}^2 (-1)^i m_b M_{\tilde{g}} s_{2\tilde{b}} \{C_0 + C_{12}\} \left(M_{\tilde{b}_i}^2 \right) \tag{68}
\end{aligned}$$

where $C_{0,11,12,23,24} \left(M_{\tilde{b}_i}^2 \right) \equiv C_{0,11,12,23,24} \left(0, 0, s; M_{\tilde{g}}^2, M_{\tilde{g}}^2, M_{\tilde{b}_i}^2 \right)$.

The vertex functions of Fig. 14:

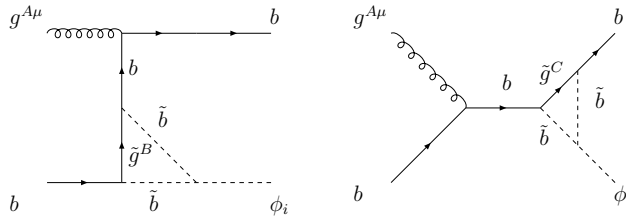


FIG. 14: Virtual diagrams, V_5 and V_6 .

Diagram V_5 :

$$\begin{aligned}
X_{V_5}^{(t)} &= \frac{4}{3} \sum_{i,j=1}^2 C_{h,ij} \{ \delta_{ij} m_b C_{11} + a_{ij} M_{\tilde{g}} C_0 \} \left(M_{\tilde{b}_i}^2, M_{\tilde{b}_j}^2 \right) \\
X_{V_5}^{(2)} &= \frac{4}{3} m_b \sum_{i,j=1,2} C_{h,ij} \delta_{ij} C_{12} \left(M_{\tilde{b}_i}^2, M_{\tilde{b}_j}^2 \right)
\end{aligned} \tag{69}$$

where $C_{0,11,12,23,24} \left(M_{\tilde{b}_i}^2, M_{\tilde{b}_j}^2 \right) \equiv C_{0,11,12,23,24} \left(0, M_h^2, t; M_{\tilde{g}}^2, M_{\tilde{b}_i}^2, M_{\tilde{b}_j}^2 \right)$, the squark mixing matrix is defined,

$$\begin{pmatrix} a_{11} & a_{12} \\ a_{21} & a_{22} \end{pmatrix} = \begin{pmatrix} s_{2\tilde{b}} & c_{2\tilde{b}} \\ c_{2\tilde{b}} & -s_{2\tilde{b}} \end{pmatrix} \tag{70}$$

and the light Higgs-squark-squark couplings $C_{h,ij}$, are normalized with respect to the Higgs-quark-quark coupling[2],

$$C_{h,11} + C_{h,22} = 4m_b + \frac{2M_Z^2}{m_b} I_3^b \frac{s_{\alpha+\beta} c_\beta}{s_\alpha} \tag{71}$$

$$C_{h,11} - C_{h,22} = 2Y_b s_{2\tilde{b}} + \frac{2M_Z^2}{m_b} c_{2\tilde{b}} (I_3^b - 2Q_b s_W^2) \frac{s_{\alpha+\beta} c_\beta}{s_\alpha} \tag{72}$$

$$C_{h,12} = C_{h,21} = Y_b c_{2\tilde{b}} - \frac{M_Z^2}{m_b} s_{2\tilde{b}} (I_3^b - 2Q_b s_W^2) \frac{s_{\alpha+\beta} c_\beta}{s_\alpha}, \tag{73}$$

$s_W^2 = \sin^2 \theta_W = 1 - M_W^2/M_Z^2$ and Y_b is defined below Eq. 41.

Diagram V_6 :

$$\begin{aligned}
X_{V_6}^{(s)} &= \frac{4}{3} \sum_{i,j=1,2} C_{h,ij} \{ \delta_{ij} m_b C_{11} + a_{ij} M_{\tilde{g}} C_0 \} \left(M_{\tilde{b}_i}^2, M_{\tilde{b}_j}^2 \right) \\
X_{V_6}^{(2)} &= \frac{4}{3} m_b \sum_{i,j=1,2} C_{h,ij} \delta_{ij} C_{12} \left(M_{\tilde{b}_i}^2, M_{\tilde{b}_j}^2 \right) \\
X_{V_6}^{(t)} &= X_{V_6}^{(3)} = X_{V_6}^{(4)} = 0
\end{aligned} \tag{74}$$

where $C_{0,11,12,23,24} \left(M_{\tilde{b}_i}^2, M_{\tilde{b}_j}^2 \right) \equiv C_{0,11,12,23,24} \left(0, M_h^2, s; M_{\tilde{g}}^2, M_{\tilde{b}_i}^2, M_{\tilde{b}_j}^2 \right)$.

The box diagram of Fig. 15:

$$\begin{aligned}
X_{B_1}^{(s)} &= \frac{3M_{\tilde{g}} s}{2} \sum_{i,j=1,2} a_{ij} C_{h,ij} \{ D_0 + D_{13} \} \left(M_{\tilde{b}_i}^2, M_{\tilde{b}_j}^2 \right) \\
X_{B_1}^{(t)} &= -\frac{3M_{\tilde{g}} t}{2} \sum_{i,j=1,2} a_{ij} C_{h,ij} D_{13} \left(M_{\tilde{b}_i}^2, M_{\tilde{b}_j}^2 \right) \\
X_{B_1}^{(1)} &= 3M_{\tilde{g}} u \sum_{i,j=1,2} a_{ij} C_{h,ij} \{ D_{11} - D_{13} \} \left(M_{\tilde{b}_i}^2, M_{\tilde{b}_j}^2 \right) \\
X_{B_1}^{(2)} &= -\frac{3m_b}{2} \sum_{i,j=1,2} \delta_{ij} C_{h,ij} \{ M_{\tilde{g}}^2 D_0 - 2D_{00} \} \left(M_{\tilde{b}_i}^2, M_{\tilde{b}_j}^2 \right)
\end{aligned} \tag{75}$$

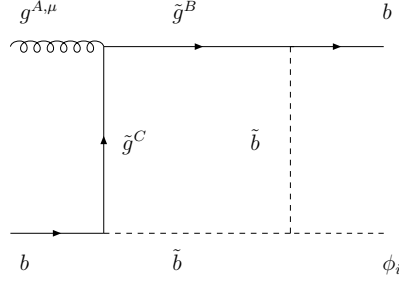


FIG. 15: Box diagram, B_1 .

where, $D_0 \left(M_{\tilde{b}_i}^2, M_{\tilde{b}_j}^2 \right) \equiv D_0 \left(0, 0, 0, M_h^2, s, t; M_{\tilde{b}_i}^2, M_{\tilde{g}}^2, M_{\tilde{g}}^2, M_{\tilde{b}_j}^2 \right)$.

The box diagram of Fig. 16:

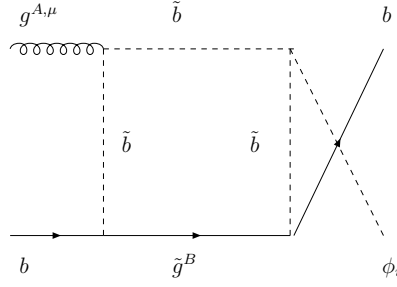


FIG. 16: Box diagram, B_2 .

Diagram B_2 :

$$\begin{aligned}
 X_{B_2}^{(s)} &= -\frac{M_{\tilde{g}} s}{6} \sum_{i,j=1,2} a_{ij} C_{h,ij} \{D_0 + D_{11}\} \left(M_{\tilde{b}_i}^2, M_{\tilde{b}_j}^2 \right) \\
 X_{B_2}^{(t)} &= \frac{M_{\tilde{g}} t}{6} \sum_{i,j=1,2} a_{ij} C_{h,ij} \{D_0 + D_{11}\} \left(M_{\tilde{b}_i}^2, M_{\tilde{b}_j}^2 \right) \\
 X_{B_2}^{(1)} &= \frac{M_{\tilde{g}} u}{3} \sum_{i,j=1,2} a_{ij} C_{h,ij} \{D_{11} - D_{12}\} \left(M_{\tilde{b}_i}^2, M_{\tilde{b}_j}^2 \right) \\
 X_{B_2}^{(2)} &= -\frac{m_b}{3} \sum_{i,j=1,2} \delta_{ij} C_{h,ij} D_{00} \left(M_{\tilde{b}_i}^2, M_{\tilde{b}_j}^2 \right)
 \end{aligned} \tag{76}$$

where $D_0 \left(M_{\tilde{b}_i}^2, M_{\tilde{b}_j}^2 \right) \equiv D_0 \left(0, 0, 0, M_h^2, u, s; M_{\tilde{b}_i}^2, M_{\tilde{g}}^2, M_{\tilde{b}_j}^2, M_{\tilde{b}_j}^2 \right)$.

The box diagram of Fig. 17:

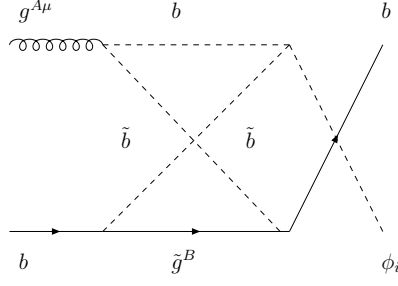


FIG. 17: Box diagram, B_3 .

Diagram B_3 :

$$\begin{aligned}
X_{B_3}^{(s)} &= \frac{M_{\tilde{g}} s}{6} \sum_{i,j=1,2} a_{ij} C_{h,ij} \{D_0 + D_{12}\} (M_{\tilde{b}_i}^2, M_{\tilde{b}_j}^2) \\
X_{B_3}^{(t)} &= -\frac{M_{\tilde{g}} t}{6} \sum_{i,j=1,2} a_{ij} C_{h,ij} \{D_0 + D_{12}\} (M_{\tilde{b}_i}^2, M_{\tilde{b}_j}^2) \\
X_{B_3}^{(1)} &= \frac{M_{\tilde{g}} u}{3} \sum_{i,j=1,2} a_{ij} C_{h,ij} \{D_{11} - D_{12}\} (M_{\tilde{b}_i}^2, M_{\tilde{b}_j}^2) \\
X_{B_3}^{(2)} &= -\frac{m_b}{3} \sum_{i,j=1,2} \delta_{ij} C_{h,ij} D_{00} (M_{\tilde{b}_i}^2, M_{\tilde{b}_j}^2)
\end{aligned} \tag{77}$$

where $D_0 (M_{\tilde{b}_i}^2, M_{\tilde{b}_j}^2) \equiv D_0 (0, 0, 0, M_h^2, u, t; M_{\tilde{b}_i}^2, M_{\tilde{g}}^2, M_{\tilde{b}_j}^2, M_{\tilde{b}_j}^2)$.

The vertex and external wavefunction counter terms, Eq. 29, along with the subtraction of Eq. 32, give the counterterm of Eq. 33:

$$\begin{aligned}
X_{CT}^{(s)} &= X_{CT}^{(t)} = \left(\frac{4\pi}{\alpha_s(\mu_R)} \right) \left[\delta Z_b^V + \frac{\delta m_b}{m_b} + \delta_{CT} \right] \\
&= \frac{4}{3} \left[2M_{\tilde{g}} Y_b I(M_{\tilde{b}_1}, M_{\tilde{b}_2}, M_{\tilde{g}}) + \sum_{i=1}^2 \left(-(-1)^i 2m_b s_{2\tilde{b}} B'_0 + 2m_b^2 B'_1 \right) (0; M_{\tilde{g}}^2, M_{\tilde{b}_i}^2) \right]
\end{aligned} \tag{78}$$

Note that the counterterm contains no large $\tan\beta$ enhanced contribution.

Appendix C: Definitions

In this appendix we define the f functions used in the expansions of the Passarino-Veltman integrals in the maximum and minimum mixing scenarios, where $R \equiv \frac{M_{\tilde{g}}}{M_S}$ in the maximal

mixing scenario, and $R_i \equiv \frac{M_{b_i}}{M_S}$ in the minimal mixing scenario:

$$\begin{aligned}
f_1(R) &= \frac{2}{(1-R^2)^2} [1 - R^2 + R^2 \log R^2] \\
f_2(R) &= \frac{3}{(1-R^2)^3} [1 - R^4 + 2R^2 \log R^2] \\
f_3(R) &= \frac{4}{(1-R^2)^4} \left[1 + \frac{3}{2}R^2 - 3R^4 + \frac{1}{2}R^6 + 3R^2 \log R^2 \right] \\
f_4(R) &= \frac{5}{(1-R^2)^5} \left[\frac{1}{2} - 4R^2 + 4R^6 - \frac{1}{2}R^8 - 6R^4 \log R^2 \right] \\
h_1(R_1, R_2, n) &= \left(\frac{R_1^2}{1-R_1^2} \right)^n \frac{\log R_1^2}{1-R_1^2} - \left(\frac{R_2^2}{1-R_2^2} \right)^n \frac{\log R_2^2}{1-R_2^2} \\
&\quad - \sum_{j=0}^n (-1)^j \frac{j+2}{2} \left\{ (1-R_1^2)^{j-n} - (1-R_2^2)^{j-n} \right\} \\
h_2(R_1, R_2) &= \frac{R_1^2 + R_2^2 - 2}{(1-R_1^2)(1-R_2^2)} + \frac{1}{R_1^2 - R_2^2} \left[\frac{R_1^2 + R_2^2 - 2R_1^4}{(1-R_1^2)^2} \log R_1^2 \right. \\
&\quad \left. - \frac{R_1^2 + R_2^2 - 2R_2^4}{(1-R_2^2)^2} \log R_2^2 \right]. \tag{79}
\end{aligned}$$

Further,

$$\begin{aligned}
f'_i(R) &\equiv \left. \frac{df_i(x)}{dx^2} \right|_{x=R} \\
f_i^{-1}(R) &\equiv \frac{f_i(1/R)}{R^2} \\
\hat{f}_i(R) &\equiv \left. \frac{1}{R^4} \frac{df_i(x)}{dx^2} \right|_{x=1/R}. \tag{80}
\end{aligned}$$

-
- [1] A. Djouadi (2005), hep-ph/0503173.
 - [2] J. F. Gunion, H. E. Haber, G. L. Kane, and S. Dawson, *THE HIGGS HUNTER'S GUIDE* (Addison Wesley (Menlo Park), 1990).
 - [3] M. S. Carena and H. E. Haber, Prog. Part. Nucl. Phys. **50**, 63 (2003), hep-ph/0208209.
 - [4] D. Benjamin et al. (Tevatron New Phenomena and Higgs Working Group) (2010), 1003.3363.
 - [5] S. Chatrchyan et al. (CMS) (2011), 1104.1619.
 - [6] G. Aad et al. (The ATLAS) (2009), 0901.0512.
 - [7] G. L. Bayatian et al. (CMS), J. Phys. **G34**, 995 (2007).

- [8] S. Dawson, C. B. Jackson, L. Reina, and D. Wackerroth, *Phys. Rev. Lett.* **94**, 031802 (2005), hep-ph/0408077.
- [9] S. Dawson, C. B. Jackson, L. Reina, and D. Wackerroth, *Mod. Phys. Lett.* **A21**, 89 (2006), hep-ph/0508293.
- [10] M. S. Carena, A. Menon, and C. E. M. Wagner, *Phys. Rev.* **D76**, 035004 (2007), arXiv:0704.1143 [hep-ph].
- [11] J. Campbell et al. (2004), hep-ph/0405302.
- [12] S. Dittmaier, M. Kramer, and M. Spira, *Phys. Rev.* **D70**, 074010 (2004), hep-ph/0309204.
- [13] M. S. Carena, S. Mrenna, and C. E. M. Wagner, *Phys. Rev.* **D60**, 075010 (1999), hep-ph/9808312.
- [14] S. Dawson, C. B. Jackson, L. Reina, and D. Wackerroth, *Phys. Rev.* **D69**, 074027 (2004), hep-ph/0311067.
- [15] F. Maltoni, Z. Sullivan, and S. Willenbrock, *Phys. Rev.* **D67**, 093005 (2003), hep-ph/0301033.
- [16] F. Maltoni, T. McElmurry, and S. Willenbrock, *Phys. Rev.* **D72**, 074024 (2005), hep-ph/0505014.
- [17] D. Dicus, T. Stelzer, Z. Sullivan, and S. Willenbrock, *Phys. Rev.* **D59**, 094016 (1999), hep-ph/9811492.
- [18] J. Campbell, R. K. Ellis, F. Maltoni, and S. Willenbrock, *Phys. Rev.* **D67**, 095002 (2003), hep-ph/0204093.
- [19] S. Dittmaier et al. (LHC Higgs Cross Section Working Group) (2011), 1101.0593.
- [20] B. Field, L. Reina, and C. B. Jackson, *Phys. Rev.* **D76**, 074008 (2007), 0705.0035.
- [21] S. Dawson and P. Jaiswal, *Phys. Rev.* **D81**, 073008 (2010), 1002.2672.
- [22] M. Beccaria et al., *Phys. Rev.* **D82**, 093018 (2010), 1005.0759.
- [23] S. Dawson and C. B. Jackson, *Phys. Rev.* **D77**, 015019 (2008), 0709.4519.
- [24] A. Dabelstein, *Nucl. Phys.* **B456**, 25 (1995), hep-ph/9503443.
- [25] L. J. Hall, R. Rattazzi, and U. Sarid, *Phys. Rev.* **D50**, 7048 (1994), hep-ph/9306309.
- [26] M. S. Carena, D. Garcia, U. Nierste, and C. E. M. Wagner, *Nucl. Phys.* **B577**, 88 (2000), hep-ph/9912516.
- [27] J. Guasch, P. Hafziger, and M. Spira, *Phys. Rev.* **D68**, 115001 (2003), hep-ph/0305101.
- [28] H. E. Haber et al., *Phys. Rev.* **D63**, 055004 (2001), hep-ph/0007006.
- [29] R. V. Harlander and W. B. Kilgore, *Phys. Rev.* **D68**, 013001 (2003), hep-ph/0304035.

- [30] S. Heinemeyer, W. Hollik, H. Rzehak, and G. Weiglein, *Eur. Phys. J.* **C39**, 465 (2005), hep-ph/0411114.
- [31] A. Brignole, G. Degrassi, P. Slavich, and F. Zwirner, *Nucl. Phys.* **B643**, 79 (2002), hep-ph/0206101.
- [32] D. Noth and M. Spira (2010), 1001.1935.
- [33] D. Noth and M. Spira, *Phys. Rev. Lett.* **101**, 181801 (2008), 0808.0087.
- [34] S. Heinemeyer, W. Hollik, and G. Weiglein, *Comput. Phys. Commun.* **124**, 76 (2000), hep-ph/9812320.
- [35] G. Degrassi, S. Heinemeyer, W. Hollik, P. Slavich, and G. Weiglein, *Eur. Phys. J.* **C28**, 133 (2003), hep-ph/0212020.
- [36] S. Heinemeyer, W. Hollik, and G. Weiglein, *Eur. Phys. J.* **C9**, 343 (1999), hep-ph/9812472.
- [37] S. Dittmaier, M. Kramer, A. Muck, and T. Schluter, *JHEP* **03**, 114 (2007), hep-ph/0611353.
- [38] M. S. Carena, M. Olechowski, S. Pokorski, and C. E. M. Wagner, *Nucl. Phys.* **B426**, 269 (1994), hep-ph/9402253.
- [39] S. Dittmaier, M. Kramer, M. Spira, and M. Walser (2009), 0906.2648.
- [40] E. L. Berger, T. Han, J. Jiang, and T. Plehn, *Phys. Rev.* **D71**, 115012 (2005), hep-ph/0312286.
- [41] L. Hofer, U. Nierste, and D. Scherer, *JHEP* **10**, 081 (2009), 0907.5408.
- [42] E. Accomando, G. Chachamis, F. Fugel, M. Spira, and M. Walser (2011), 1103.4283.
- [43] S. Berge, W. Hollik, W. M. Mosle, and D. Wackerroth, *Phys. Rev.* **D76**, 034016 (2007), hep-ph/0703016.
- [44] P. Nason, S. Dawson, and R. K. Ellis, *Nucl. Phys.* **B303**, 607 (1988).
- [45] J. F. Gunion, H. E. Haber, and M. Sher, *Nucl. Phys.* **B306**, 1 (1988).
- [46] P. M. Nadolsky et al., *Phys. Rev.* **D78**, 013004 (2008), 0802.0007.
- [47] A. D. Martin, W. J. Stirling, R. S. Thorne, and G. Watt, *Eur. Phys. J.* **C63**, 189 (2009), 0901.0002.